Ocean Processes Affecting the Twenty-First-Century Shift in ENSO SST Variability

CONG GUAN

Key Laboratory of Ocean Circulation and Waves, Institute of Oceanology, Chinese Academy of Sciences, Qingdao, and University of Chinese Academy of Sciences, Beijing, China, and NOAA/Pacific Marine Environmental Laboratory, Seattle, Washington

MICHAEL J. MCPHADEN

NOAA/Pacific Marine Environmental Laboratory, Seattle, Washington

(Manuscript received 8 December 2015, in final form 24 June 2016)

ABSTRACT

Sea surface temperature (SST) variability associated with El Niño–Southern Oscillation (ENSO) slightly increased in the central Pacific Ocean but weakened significantly in the eastern Pacific at the beginning of twenty-first century relative to 1980–99. This decadal shift led to the greater prominence central Pacific (CP) El Niño events during the 2000s relative to the previous two decades, which were dominated by eastern Pacific (EP) events. To expand upon previous studies that have examined this shift in ENSO variability, temperature and temperature variance budgets are examined in the mixed layer of the Niño-3 (5°S–5°N, 150°–90°W) and Niño-4 (5°S–5°N, 160°E–150°W) regions from seven ocean model products spanning the period 1980–2010. This multimodel-product-based approach provides a robust assessment of dominant mechanisms that account for decadal changes in two key index regions. A temperature variance budget perspective on the role of thermocline feedbacks in the ENSO cycle based on recharge oscillator theory is also presented. As found in previous studies, thermocline and zonal advective feedbacks are the most important positive feedbacks for generating ENSO SST variance, and thermodynamic damping is the largest negative feedback for damping ENSO variance. Consistent with the shift toward more CP El Niños after 2000, thermocline feedbacks experienced a substantial reduction from 1980 to 1999 and into the 2000s, while zonal advective feedbacks were less affected. Negative feedbacks likewise weakened after 2000, particularly thermal damping in the Niño-3 region and the nonlinear sink of variance in both regions.

1. Introduction

The El Niño–Southern Oscillation (ENSO) phenomenon is the most prominent interannual climate fluctuation on the planet, affecting patterns of weather variability worldwide (McPhaden et al. 2006). The warm phase of ENSO, known as El Niño, is associated with weakened trade winds and warm sea surface temperature (SST) anomalies in the equatorial Pacific Ocean, and the converse for its cold counterpart, La Niña. El Niño and La Niña are controlled by a delicate balance of positive and negative feedbacks that either amplify or damp the ENSO anomalies. According to Jin et al. (2006), key positive feedbacks determining ENSO event growth include the Bjerknes feedback between zonal wind stress and SST, the thermocline feedback (TCF) associated with equatorial thermocline depth variations and its effects on SST, the zonal advective feedback (ZAF) that results from anomalous zonal current advection of SST, and the Ekman feedback (EKF) associated with local wind-driven anomalous vertical advection of temperature. Net surface heat flux is, on the other hand, typically the largest negative feedback that acts to damp SST anomalies.

Recently, a new type of El Niño has been detected, with maximum warm SST anomalies centered near the date line. This type of El Niño has been called a central Pacific (CP) El Niño (Kao and Yu 2009), date line El Niño (Larkin and Harrison 2005a,b), El Niño Modoki

Pacific Marine Environmental Laboratory contribution number 4411.

Corresponding author address: Cong Guan, 7 Nanhai Road, Qingdao, Shandong 266071, China.
E-mail: guancong10@mails.ucas.ac.cn

DOI: 10.1175/JCLI-D-15-0870.1

© 2016 American Meteorological Society

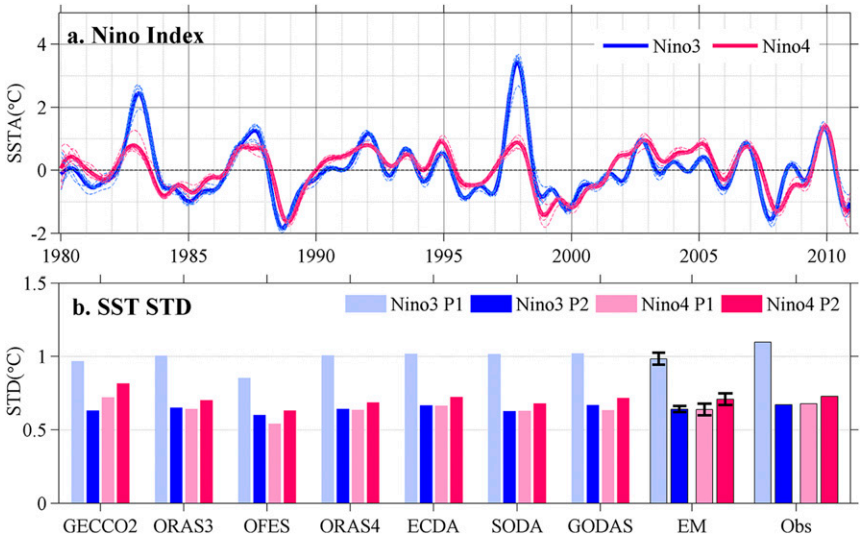

FIG. 1. Interannual SST variations in the Niño-3 and Niño-4 regions. (a) Ensemble-mean time series of Niño-3 and Niño-4 indices (thick lines) and individual time series derived from the various model products (thin dashed lines). (b) Standard deviation (STD) of interannual SST anomalies in P1 and P2 for each product in Niño-3 and Niño-4 regions. The labels EM and Obs denote the ensemble mean of the model products and observational indices from NOAA/CPC, respectively. Error bars are shown for 95% confidence intervals of EM.

(Ashok et al. 2007), or warm pool El Niño (Kug et al. 2009). The occurrence of CP El Niños has attracted a lot of scientific attention, challenging classical ENSO theories because of its distinct spatial characteristics and climate impacts that can differ from the typical eastern Pacific (EP) El Niño events (Kug et al. 2009; Ashok and Yamagata 2009). Numerous efforts have been made to examine the differences between EP and CP El Niños in terms of dynamical and thermodynamical processes (e.g., Kug et al. 2009; Ren and Jin 2013). It has been suggested that the TCF plays a dominant role in the development phases of EP El Niño events because of the shallow mean thermocline in the EP, but the ZAF are more effective in the generation of CP El Niño anomalies because of the strong SST zonal gradient in the CP (Picaut et al. 1996; Kug et al. 2009; Guan et al. 2013). Ren and Jin (2013) argued, on the other hand, that the TCF makes the largest contribution to the growth rate for CP as well as EP El Niños.

The twenty-first century has witnessed a shift in ENSO variability relative to the latter part of the twentieth century (McPhaden 2012; Hu et al. 2013; Lübbecke and McPhaden 2014, hereafter LM2014). CP El Niño events have occurred more frequently than EP El Niño events (Lee and McPhaden 2010; McPhaden 2012; Xiang et al. 2013; Wen et al. 2014), accompanied by a small increase in interannual SST variability in the Niño-4 region (5°S–5°N, 160E°–150°W) and a larger decrease in the Niño-3 region (5°S–5°N, 150°–90°W) in the 2000s (Figs. 1 and 2). At the same time, ENSO predictability has also decreased (Barnston et al. 2012; McPhaden 2012; Horii et al. 2012). It is of fundamental importance to clarify why these changes in the ENSO cycle have occurred and what processes account for them because of the implications these changes have for seasonal predictability and prediction.

To verify what accounts for this twenty-first-century shift in ENSO characteristics, LM2014 assessed ENSO feedbacks based on the Bjerknes stability index (BJ index; Jin et al. 2006). They found that a weakened TCF leads to a decrease of ENSO variability in EP in the 2000s relative to the 1980s–90s because of a reduced response of thermocline slope to zonal wind stress anomalies and the response of wind stress to eastern equatorial Pacific SST anomalies. However, the BJ index methodology does not allow for a detailed examination of the spatial variability of various feedbacks, therefore how the ZAF changed farther to the west, where it has larger amplitude and is important in the development of CP El Niños (e.g., Kug et al. 2009; Chung and Li 2013; Guan et al. 2013), could not be thoroughly examined. Furthermore, Graham et al. (2014) pointed out that the BJ index overestimates the relative importance of the TCF to the ZAF and also overlooks nonlinearities in the surface layer heat balance.

In terms of decadal changes in ENSO variability, Dewitte et al. (2013) suggested that TCF becomes more

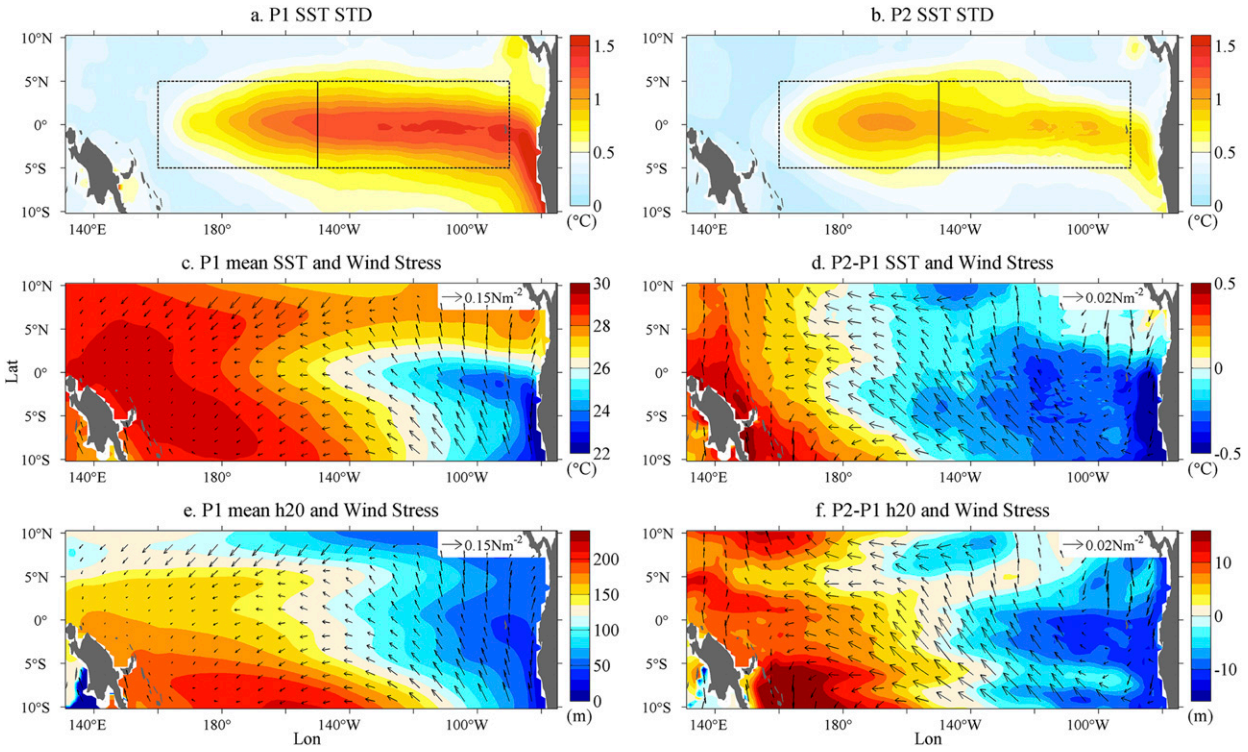

FIG. 2. Standard deviation of interannual SST anomalies during (a) P1 and (b) P2. (c) Mean SST and (e) depth of the 20°C isotherm with wind stress (vectors) overlaid for P1 and (d),(f) the differences between P2 and P1. Figures are based on the reanalysis ORAS3, which is similar to other observations and model products used in this study.

effective in the western-central equatorial Pacific after the 1976 shift as a result of increased stratification. Recently, Boucharel et al. (2015) found that the TCF and the dynamical damping account for most of the multidecadal ENSO variance across the equatorial Pacific, based on a variance heat budget (Santoso et al. 2010). Thus, while there is general agreement that the TCF is the most effective positive feedback in the eastern Pacific, the relative contributions of the ZAF and TCF in the central Pacific between the end of the twentieth century and beginning of the twenty-first century is less clear and still needs to be addressed.

Moreover, according to the recharge–discharge oscillator by Jin (1997a,b), the TCF affects not only the growth rate of ENSO anomalies, but also the switch in ENSO phase between El Niño and La Niña. Ren and Jin (2013) found that the TCF contributes the most to recharge–discharge processes throughout the life cycles of both CP and EP ENSO types. Conversely, Kug et al. (2009, 2010) argued that the TCF is effective during the transition phase of EP events, but the classical recharge oscillator does not work as well for CP El Niño events. Thus, it is also important to consider how possible changes of these feedbacks might explain the details of ENSO phase transitions in the twenty-first century dominated by CP El Niños versus transitions in the 1980s–90s dominated by EP El Niños.

Graham et al. (2014) argued that there are advantages to directly computing the mixed layer temperature balance over using the more approximate BJ index as in LM2014 for assessing various feedback processes involved in ENSO evolution. In the present paper, we will therefore examine both the temperature budget and the temperature variance budget for 1980–99 and 2000–10 separately to directly describe how each dynamical process changed between the twentieth and the twenty-first century in the equatorial Pacific. We focus on the Niño-3 and Niño-4 regions that encompass the areas of maximum interannual SST variance during the 1980s–90s and 2000s respectively (Fig. 2). Our temperature variance budget calculation is similar to that of Boucharel et al. (2015), but unlike Boucharel et al. (2015), we retain the time-dependent term and explicit representation of surface fluxes in our diagnostic framework in order to provide a clearer definition of positive and negative feedbacks over the course of individual ENSO events. Our methodology will provide a clearer picture of spatial variations in the important feedbacks than LM2014 were able to discern using the BJ index.

Data and methodology will be described in section 2, followed by an investigation of the twenty-first-century shift of ENSO variability in section 3, with emphasis on clarifying the role of major feedbacks based on the temperature variance budget. Section 4 will summarize the results and discuss remaining issues.

2. Data and methods

a. Ocean data, reanalysis, and simulation products

Six ocean reanalysis products and one simulation without data assimilation are used in this study. The reanalyses include the German contribution to Estimating the Circulation and Climate of the Ocean, version 2 (GECCO2; Köhl and Stammer 2008), from Hamburg University; the Ocean Reanalysis System, versions 3 (ORAS3; Balmaseda et al. 2008) and 4 (ORAS4; Balmaseda et al. 2013), from the European Centre for Medium-Range Weather Forecasts (ECMWF); the latest version of the Simple Ocean Data Assimilation (SODA2.2.4; Carton and Giese 2008); the ensemble coupled data assimilation (ECDA) product from the Geophysical Fluid Dynamics Laboratory (GFDL ECDA3.1; Zhang et al. 2007); and the Global Ocean Data Assimilation System (GODAS; Behringer and Xue 2004) from the NOAA/Climate Prediction Center (CPC). The simulation is from the Ocean GCM for the Earth Simulator (OFES; Masumoto et al. 2004) based on MOM, version 3.0 (MOM 3.0). Collectively, we will refer to these as model products, detailed descriptions of which can be found in Table 1 and also from the Asia–Pacific Data-Research Center at the University of Hawai'i (http://apdrc.soest.hawaii.edu/data/data.php).

Monthly averaged fields of ocean temperature, three-dimensional ocean current velocities (u, v, and w), and surface heat flux q_{net} are extracted from these products for the temperature budget and temperature variance budget calculations. For those products without vertical velocity fields provided (GODAS, ORAS4, and GFDL ECDA3.1), we calculate vertical velocity based on mass continuity: $w = -\int_{z=-h}^{0} \nabla_h \cdot \mathbf{v}\, dz$, where $w(0) = 0$ and $\mathbf{v}$ is the horizontal velocity vector. As for ORAS4 and SODA2.2.4, sea surface net heat fluxes are taken from atmospheric inputs that are used to force the corresponding ocean model [i.e., ERA-40 (1980–89) and ERA-Interim (1989–2009) for ORAS4 and NOAA 20CR, version 2 (20CRv2) for SODA2.2.4]. Each ocean model product covers the period from January 1980 to December 2010. We will use ORAS3 as a representative ocean analysis to illustrate certain aspects of the variability in greater detail. We have extracted the 20°C isotherm depth (h20) as an index describing the thermocline depth in this model product in order to analyze TCF changes associated with the recharge oscillator.

The Niño-3 and Niño-4 indices provided by the NOAA/Climate Predict Center (http://www.cpc.noaa.gov/products/analysis_monitoring/ensostuff/ensoyears.shtml) are also used in this paper to compare with results from the model products. These indices are obtained from the 3-month running mean of ERSST version 4 (Huang et al. 2015) in situ monthly SST anomalies centered on 30-yr base periods updated every 5 yr. The SST data are on a $2° \times 2°$ grid and derived from ICOADS release 2.5 from 1875 to 2007 (Woodruff et al. 2011) and after 2007 from Global Telecommunications System (GTS) receipts from the National Centers for Environmental Prediction (NCEP).

b. Methods

A temperature budget analysis is first carried out for the Niño-3 and Niño-4 regions with a fixed bottom as 50-m depth, following Lee et al. (2004) and Zhang and McPhaden (2010, hereafter ZM2010). The mixed-layer temperature balance can be expressed as

$$\begin{aligned}\text{MLT}_t = {} & T_{\text{advB}} + T_{\text{advW}} + T_{\text{advE}} + T_{\text{advS}} + T_{\text{advN}} \\ & + T_{\text{surf}} + R, \end{aligned} \tag{1}$$

where MLT_t represents the time tendency of box-mean mixed layer temperature (MLT; i.e., $T_{\text{ave}} = B^{-1}\iiint_B T\, dx\, dy\, dz$), and T_{surf} is proportional to the net surface heat flux q_{net} [i.e., $T_{\text{surf}} = (\rho c_p B)^{-1}\iint q_{\text{net}}\, dx\, dy$, where ρ is density, c_p is heat capacity, and B is volume]. Here ρ and c_p are respectively constants $1022.6\,\text{kg}\,\text{m}^{-3}$ and $3940\,\text{J}\,\text{kg}^{-1}\,\text{K}^{-1}$. Advection across the five interior ocean interfaces of the box is denoted T_{advB} (for bottom) and T_{advW}, T_{advE}, T_{advS}, and T_{advN} (for western, eastern, southern, and northern boundaries, respectively). Advection terms are defined as $T_{\text{adv}i} = B^{-1}\int_A (\mathbf{V}\cdot\mathbf{n})\delta T_i\, dS$, where i denotes various boundaries, S denotes corresponding interfacial area, and $\mathbf{V}\cdot\mathbf{n}$ is the normal velocity at each interface. Temperature difference δT_i represents the difference between the interface temperature T_i and the MLT (i.e., $\delta T_i = T_i - T_{\text{ave}}$). Thus, these advection terms represent the advection of interfacial temperature relative to the volume averaged temperature of the box by inflow normal to the interface. Since the Niño-3 region has a larger horizontal area than the Niño-4 region, we normalize each term by its corresponding volume B for ease of comparisons between two regions. Heat redistributed internally by small-scale processes inside the box does not affect the tendency of the

TABLE 1. Detailed specifications of the model products used in this paper. (Additional acronym expansions are available at http://www.ametsoc.org/PubsAcronymList.)

Datasets	Horizontal resolution (lon × lat)	Models	Assimilation method	Forcing and relaxation used	Available variables
GECCO2	1° × 1/3°	MITgcm	Four-dimensional variational data assimilation (4D-VAR) (adjoint) method	NCEP–NCAR reanalysis (R1) atmospheric fields and bulk formulas.	T, u, v, w, and q_{net}
ORAS3	1.4063° × 0.3°	HOPE	Multivariate optimum interpolation (OI) with bias correction	ERA-40 daily fluxes from 1959 to 2002. ECMWF operational NWP fluxes (2003–11); ERA-40 SST (1959–82) and weekly NOAA OISSTv2 (1982–2011). ERA-40 is directly assimilated with raw (level 1b) TIROS Operational Vertical Sounder (TOVS) data from October 1978 to December 2002.	T, u, v, w, and q_{net}
ORAS4	1° × 1°	NEMO, version 3.0	NEMO variational data assimilation (NEMOVAR) in its 3D variational data assimilation the first-guess at appropriate time (FGAT) mode	Daily surface fluxes of heat, freshwater and momentum and, from ERA-40 (1958–1989), ERA-Interim reanalysis (1989–2009) and ECMWF atmospheric analysis (2010–2014).	T, u, and v
SODA2.2.4	0.5° × 0.5°	POP, version 2	Ensemble Kalman filter	20CRv2 surface wind stress and heat flux determined using bulk formulas.	T, u, v, and w
ECDA3.1	1° × 1/3°	GFDL's ECDA system	Ensemble Kalman filter	Atmospheric component of the coupled model, so the heat fluxes are computed in the model system and not just subscribed from a given boundary condition as in an uncoupled case.	T, u, v, and q_{net}
GODAS	1° × 1/3°	GFDL MOM 3.0	3D variational data assimilation scheme of Derber and Rosati (1989)	Surface heat flux, freshwater flux and momentum flux from the atmospheric NCEP Reanalysis 2 (R2)	T, u, v, w, and q_{net}
OFES	0.1° × 0.1°	GFDL MOM 3.0	—	The wind stresses and surface tracer fluxes NCEP–NCAR reanalysis products. The surface heat flux is calculated by the bulk formula, using NCEP–NCAR reanalysis output.	T, u, v, w, and q_{net}

average temperature within the box (Lee et al. 2004; Kim et al. 2007) and would not affect the calculation of heat advection. Besides, effects of volume transports whose temperature is the same as the box average temperature produce no effect (ZM2010). More details can be found in Lee et al. (2004).

Our study is primarily motivated to explore the role of different feedbacks affecting the twenty-first-century shift in ENSO variability, expanding on the work of LM2014. Therefore, we used a constant mixed layer depth (MLD) of 50 m in both the Niño-3 and Niño-4 regions to make comparisons easier with previous studies that also used a constant mixed layer depth (e.g., ZM2010; LM2014; Graham et al. 2014). We find that results are not fundamentally sensitive to varying this fixed mixed layer depth by ±20 m as long as that definition leads to an MLT that is representative of SST. Other choices of mixed layer depth definition are possible: for example, MLD defined based on a vertical density change criterion that would allow the mixed layer to migrate vertically with time. However, a time-varying mixed layer, which has certain advantages in separating out diabatic and adiabatic vertical processes, would make comparison with previous results more difficult.

Horizontal and vertical diffusion, effects from high-frequency tropical instability waves, penetrative shortwave radiation through the base of the mixed layer, and computational errors and errors associated with imperfect closure of the heat budget are contained in the residual term R. The imperfect closure of the heat budget can include (i) the MLT tendency due to SST relaxation and (ii) the tendency incurred by the so-called assimilation increment, which is a statistical correction applied during sequential data assimilation time steps to correct the model state to fit the observations. These assimilation increments result in internal heat sources and sinks due at each time step. Only the free-run OFES and GECCO2, which uses an adjoint assimilation method, do not have assimilation increments. In using seven model products, each having different assimilation procedures, it is our expectation that uncertainties in any individual model result will be reduced through ensemble averaging.

To examine the individual physical feedbacks separately, we regrouped terms in the temperature balance by breaking up variables into climatological means and monthly anomalies about the mean: $M = \overline{M} + M'$, where M is MLT, ocean velocity, or another variable. For instance, anomalous T_{advB} can be divided into three parts [(2)]: anomalous temperature advection by the mean current $\overline{w_B}\delta T'_B$, which refers to the thermocline feedback; mean temperature advection by the anomalous current $w'_B\overline{\delta T_B}$, which is the Ekman feedback; and anomalous temperature advection by the anomalous current $w'_B\delta T'_B$, which is a nonlinear term:

$$T'_{\text{advB}} = \frac{1}{B}\iint (\overline{w_B}\delta T'_B + w'_B\overline{\delta T_B} + w'_B\delta T'_B)\,dx\,dy. \quad (2)$$

In this manner, we rewrite (1) to illustrate the various feedbacks as (see the appendixes)

$$\text{MLT}_t = \text{TCF} + \text{EKF} + \text{ZAF} + \text{MAF} + \text{MHD} + \text{TD} + \text{NL} + R, \quad (3)$$

where TCF, EKF, and ZAF are defined as above, and the other terms are meridional advective feedback (MAF), mean horizontal dynamical heating term (MHD), thermal damping by net surface heat flux (TD), and nonlinear advection (NL). In (3), all terms refer to anomalies and primes have been dropped for simplicity.

The feedbacks in (3) have been represented in various ways by different authors. Our definitions are similar to those in ZM2010 and Graham et al. (2014). In particular, we use δT_B in the expression for TCF to calculate net contributions of thermocline variations to MLT variance. Our definition of TCF ($B^{-1}\iint \overline{w_B}\delta T'_B\,dx\,dy$) is expressed as $\overline{w_B}[(T'_B - T'_{\text{ave}})/h]$, which includes both $\overline{w_B}(T'_B/h)$ and $-\overline{w_B}(T'_{\text{ave}}/h)$. This definition differs from that of the BJ index, where the TCF includes only the first of these terms with the second term grouped into the BJ index expression for three-dimensional mean dynamical heating. As Graham et al. (2014) showed, the two expressions for TCF are highly correlated (primarily because T'_B and T'_{ave} are highly correlated). As a consequence of grouping $-\overline{w_B}(T'_{\text{ave}}/h)$ into TCF, our definition of MHD includes only advection by mean horizontal currents, in contrast to advection by three-dimensional mean currents as in the BJ index and some other studies (e.g., An et al. 1999; Jin et al. 2006; LM2014; Boucharel et al. 2015). MAF is a relatively small term, which has been neglected or grouped into EKF in some previous studies (e.g., Jin et al. 2006; LM2014; Boucharel et al. 2015). These differences in definitions between various studies though do not obscure the fundamental dynamical and thermodynamical processes at work in the ENSO cycle, as we shall see below.

Interannual variations for each term are obtained using a Fourier low-pass filter with a cutoff period of 15 months (Walters and Heston 1982). From Fig. 3, we can see that the sum of the first seven temperature

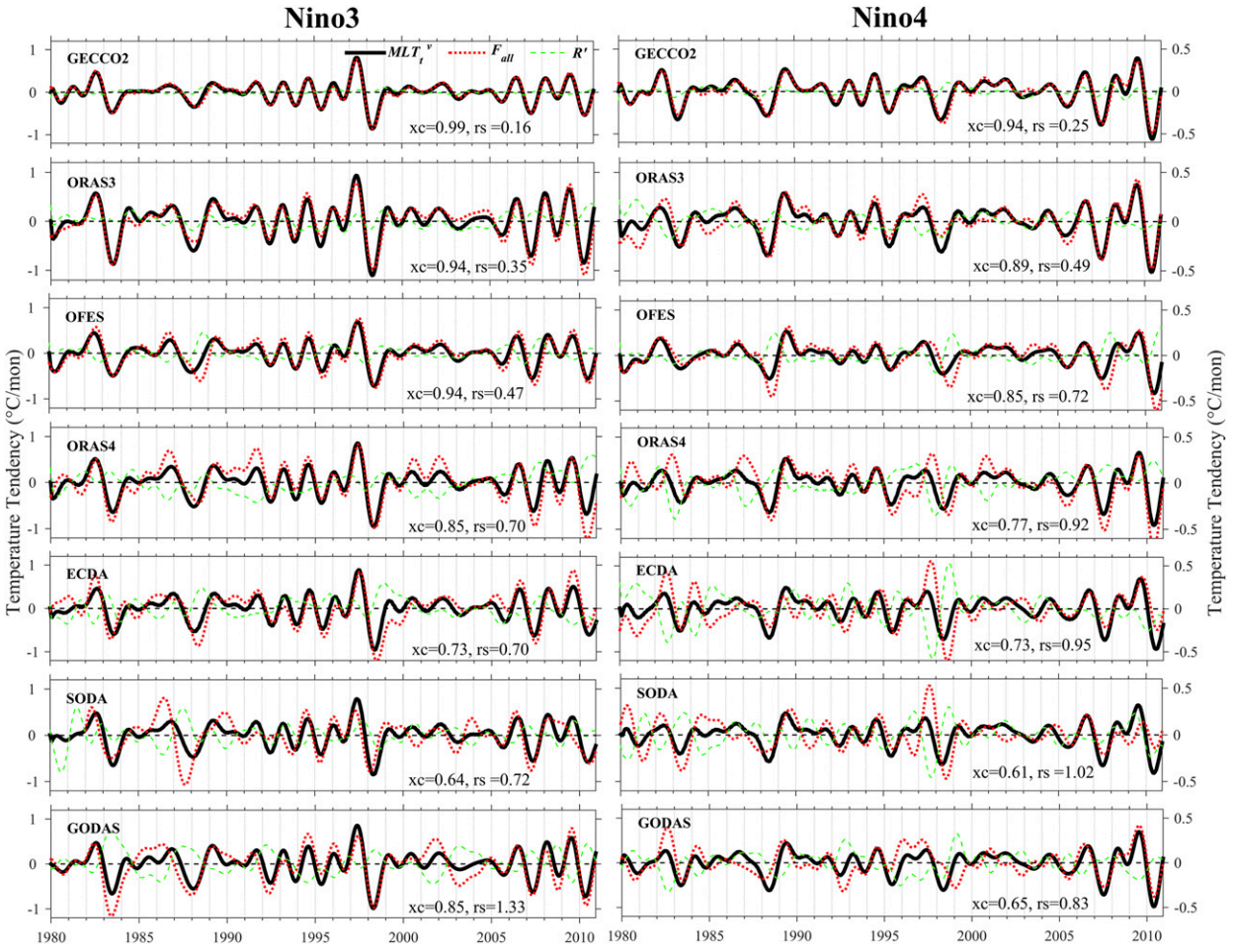

FIG. 3. Interannual anomalies (°C month^{-1}) in the mixed layer heat balance from (3): MLT$_t$ (solid black), $F_{\rm all}$ (red dotted), and residual term R (dashed green) for (top)–(bottom) each model product for (left) the Niño-3 region and (right) the Niño-4 region. The $F_{\rm all}$ is the sum of all the feedback terms on the right-hand side of (3), except for R. Cross correlation coefficients (xc) between MLT$_t$ and $F_{\rm all}$ and the ratios (rs) of STD(R)/STD(MLT$_t$) are shown in each graph. A perfect match between MLT$_t$ and $F_{\rm all}$, implying exact closure of the heat balance involving the explicitly represented terms, would have a cross correlation of unity and ratio of zero. Note the vertical scale for Niño-4 at right is smaller than for Niño-3. All correlation coefficients are significantly different from zero at the 95% confidence levels according to methods described in Dawdy and Matalas (1964) and Haan (2002).

feedback terms on the right-hand side of (3), namely $F_{\rm all}$, is highly correlated with and accounts for most of the temperature tendency, exceeding 95% significance. Among the various products, GECCO2, ORAS3, ORAS4, and OFES show the highest correlation coefficients between MLT$_t$ and $F_{\rm all}$. The highest correlation is for GECCO2, where the adjoint assimilation method is used to adjust the entire model state to improve the consistency with observations as well as prior estimates of surface fluxes, such that heat is conserved. As for the products that do not conserve heat because of the way temperature data are assimilated (e.g., SODA2.2.4, GFDL ECDA3.1, and GODAS), one should expect less exact balances and lower correlations between MLT$_t$ and $F_{\rm all}$. We also note that in general the temperature balance closes better in the Niño-3 than the Niño-4 region since SST variability is stronger in the Niño-3 region with the exception of the last 10 yr of the 30-yr record (Fig. 1). There is a tendency for the amplitude of $F_{\rm all}$ to be larger than MLT$_t$ in both regions. This tendency may result from the neglect of processes such as vertical and horizontal diffusion. It could also indicate that they tend to produce overly energetic ENSO SST variations because of model limitations and that assimilation increments, as reflected in the residuals R, correct these deficiencies to produce a more realistic ENSO SSTs.

Analysis of the temperature or heat budget has been the traditional approach for determining how various processes affect the storage of heat in the mixed layer. Santoso et al. (2010) recently suggested a complimentary methodology, namely a "temperature variance equation," obtained by multiplying the temperature balance equation by temperature anomalies. This method is able to estimate the contributions of each term to the temperature variance growth rate, and by so doing explicitly identifies when a term is a positive feedback (creating variance) or a negative feedback (damping variance). Thus, we multiply (3) by MLT anomaly $T'_{\rm ave}$ to obtain the temperature variance budget:

$$\mathrm{MLT}_t^{\upsilon} = \mathrm{TCF}^{\upsilon} + \mathrm{EKF}^{\upsilon} + \mathrm{ZAF}^{\upsilon} + \mathrm{MAF}^{\upsilon} + \mathrm{MHD}^{\upsilon} + \mathrm{NL}^{\upsilon} + \mathrm{TD}^{\upsilon} + R^{\upsilon}, \quad (4)$$

where $\mathrm{MLT}_t^{\upsilon} = T'_{\rm ave}(\partial T'_{\rm ave}/\partial t) = 0.5(\mathrm{MLT}^{\upsilon})_t$ and each feedback term is labeled with superscript υ to represent the corresponding term in the temperature budget [(3)]. The left-hand side of (4) shows the time-dependent temperature variance tendency in the mixed layer. On the right-hand side, a positive value of a component means that term represents a positive feedback on MLT variance growth, while negative values represent negative feedbacks. Specific definitions of each term in the temperature variance budget equation are shown in the appendixes.

3. Results

a. *Characterizing the twenty-first-century shift of ENSO SST variability*

As in LM2014, we define the period 1980–99 as P1 and 2000–10 as P2. Computing the standard deviations of interannual SST anomalies separately over these periods in both the Niño-3 and Niño-4 regions from various datasets (Fig. 1) shows very good agreement between the model products with themselves and with the observations. This is not surprising, since all the products (except for the simulation from OFES) assimilate observed SSTs. The shift of ENSO variability in the first decade of the twenty-first century is evident in both observations and the seven oceanic model products, with weaker interannual SST variability in the Niño-3 region (an ensemble-mean value of 0.64°C in the 2000s versus 0.98°C in the 1980s–90s) but slightly stronger interannual SST variability in the Niño-4 region (0.71°C in the 2000s relative to 0.64°C in the 1980s–90s). The spatial variability in SST standard deviation for the ORAS3 SST product during P1 and P2 (Figs. 2a,b) indicates a clear change of pattern of ENSO SST anomalies, with the largest SST variance during P1 in the Niño-3 region of the eastern equatorial Pacific but largest SST anomalies during P2 shifted westward to the Niño-4 region. This longitudinal shift in SST variance is consistent with previous studies, indicating a greater frequency of occurrence of CP El Niño events in the 2000s than in the previous two decades (Lee and McPhaden 2010; McPhaden et al. 2011; McPhaden 2012; Xiang et al. 2013).

These changes in ENSO SST variability occur in concert with changes in the background state of the tropical Pacific Ocean over the past 30 years (McPhaden et al. 2011; Chung and Li 2013). In particular, easterly zonal wind stress was enhanced in the 2000s compared to 1980–99 and accompanied by stronger zonal SST and thermocline gradients across the equatorial Pacific. We will return to a discussion of these decadal time-scale background state changes in relation to ENSO SST variations in the final section.

b. *The temperature variance budget*

The ensemble-mean time series of individual terms in both the Niño-3 and Niño-4 boxes from the seven model products (Figs. 4 and 5) show that the temperature variance tendency $\mathrm{MLT}_t^{\upsilon}$ is positive during developing phases of El Niño and La Niña events, negative during their decay phases, and zero at the peaks of events. Among the various terms in the budget, TCF^{υ}, EKF^{υ}, ZAF^{υ}, and MHD^{υ} are mostly positive (i.e., tending to generate temperature variance). Of these, TCF^{υ} and ZAF^{υ} are the largest positive terms and thus the most effective in generating ENSO variability (Kug et al. 2009; ZM2010; Ren and Jin 2013). The Ekman feedback is most effective in the Niño-3 region, particularly in the developing and decaying phases of events. It is noteworthy that TCF^{υ} and ZAF^{υ} become negative during decay phases of both warm and cold events, especially in extreme El Niño events. The implications of negative TCF^{υ} from the perspective of recharge oscillator theory will be discussed in section 3d.

The thermal damping term TD^{υ} is always negative, tending to destroy MLT variance once developed in both the Niño-3 and Niño-4 regions. Similarly, the mean horizontal dynamical term MHD^{υ} sets in only once anomalies are developed. By our definition, this is a positive feedback and mostly due to mean meridional currents acting on the surface temperature anomalies, which are largest in the center of the

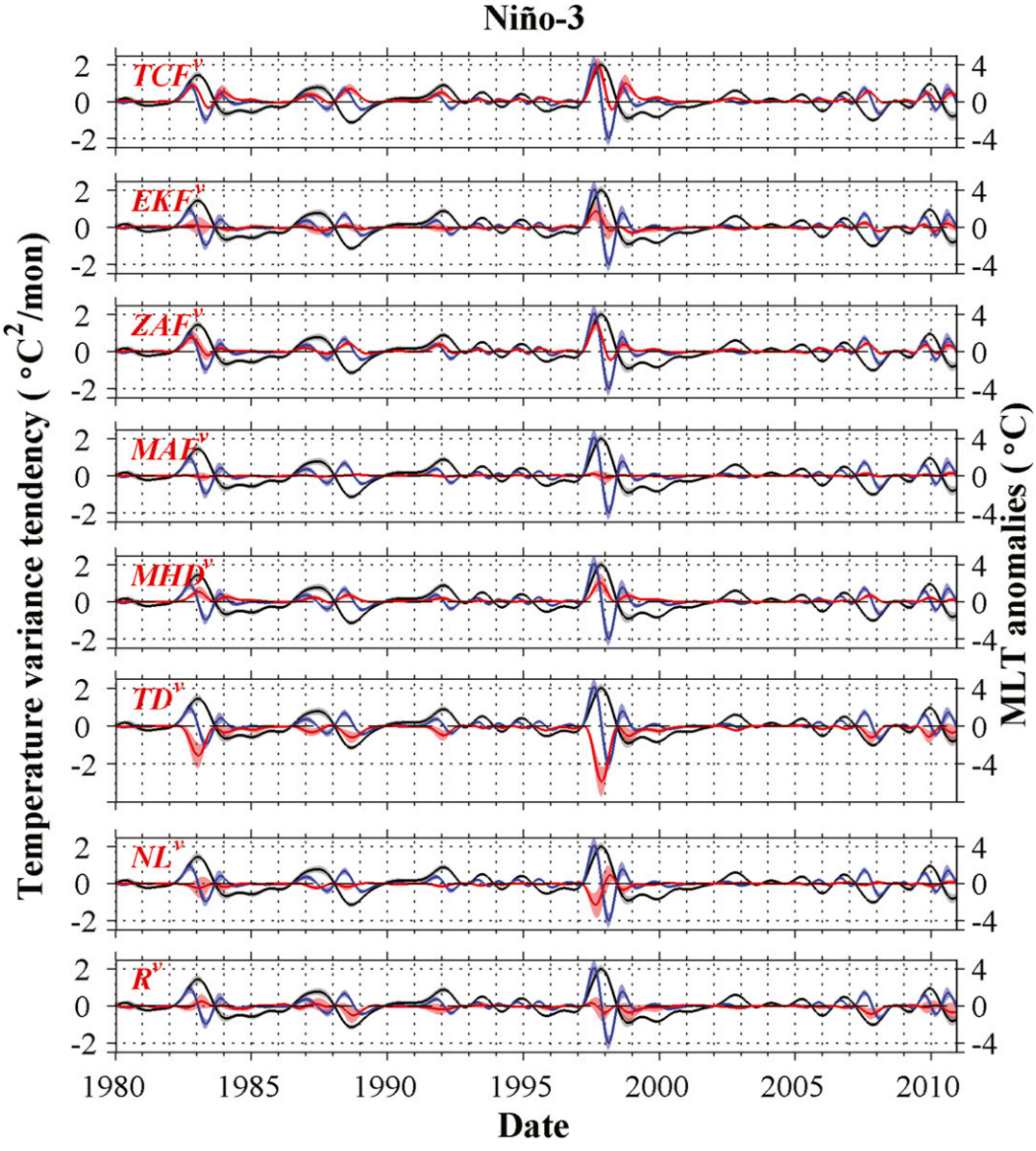

FIG. 4. Ensemble means of individual temperature variance budget terms (red lines) superimposed on the ensemble-mean MLT anomalies (black lines) and temperature variance tendency (blue lines; °C^2 month^{-1}) averaged in the Niño-3 region. Shading around the ensemble means indicates the standard deviation among different products.

Niño-3 and Niño-4 regions (Fig. 2). Climatological poleward meridional currents at the northern and southern boundaries thus advect relative weaker anomalies out of these regions, thus reinforcing box averaged MLT variance, as also shown by ZM2010 and Kug et al. (2009). The MAF^{v} in both regions is relatively small.

The nonlinear term NL^{v} is generally negative but can at times be positive, as, for example, during the decay phase of extreme events like the 1997/98 El Niño and in the Niño-4 region during P2. It is most significant in the Niño-3 region, where anomalies are largest on average, consistent with the fact that nonlinearity is proportional to squared anomaly fields. This effect of nonlinearity in our balance is different from that inferred by Jin et al. (2003), who suggested that the nonlinear terms contribute to amplifying strong warm ENSO events based on the SODA2.2.4 and GODAS products. In our analysis, however, these terms in both SODA2.2.4 (a different version than used in Jin et al.) and GODAS are negative feedbacks during the development phase of

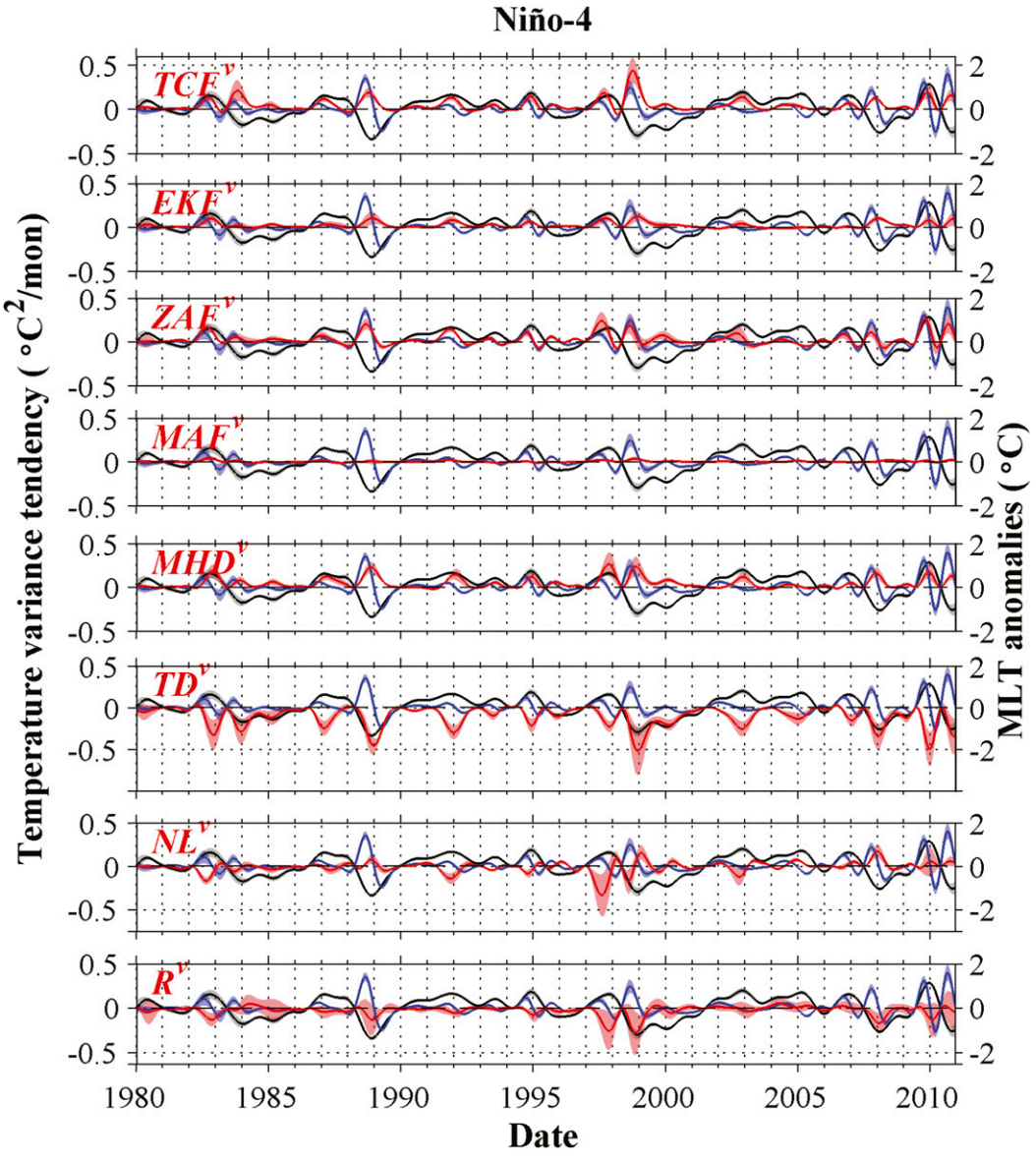

FIG. 5. As in Fig. 4, but for the Niño-4 region. Note, however, that the vertical scale is different.

ENSO events (see Fig. 7). Thus, our results suggest that the role of nonlinearity may not only be sensitive to the particular region in question and whether one considers the growth or decay phase of ENSO, but also to the particular choice of model.

Finally, the residual term R^{υ} is mostly negative in both regions and generally small compared to the largest terms (i.e.,$\mathrm{MLT}_t^{\upsilon}$, TCF^{υ}, ZAF^{υ}, and TD^{υ}). It is not well correlated with $\mathrm{MLT}_t^{\upsilon}$ or MLT^{υ} in either region, but tends to be anticorrelated with F_{all} (especially for OFES, ORAS4, GFDL ECDA3.1, SODA2.2.4, and GODAS). As discussed in relation to the heat balance (3), this tendency may result from some combination of neglected physical processes in our temperature variance formulation and from assimilation increments, as reflected in the residual R, that correct for model deficiencies to produce realistic ENSO SSTs.

Figure 6 summarizes averages of individual feedback terms over the entire 30-yr record in both Niño index regions. Following Santoso et al. (2010), we also averaged over the positive and negative values of $\mathrm{MLT}_t^{\upsilon}$ separately to distinguish between the strength of feedback tendencies during variance growth and decay phases. Thus, our method, using the MLT variance tendency as an index to examine

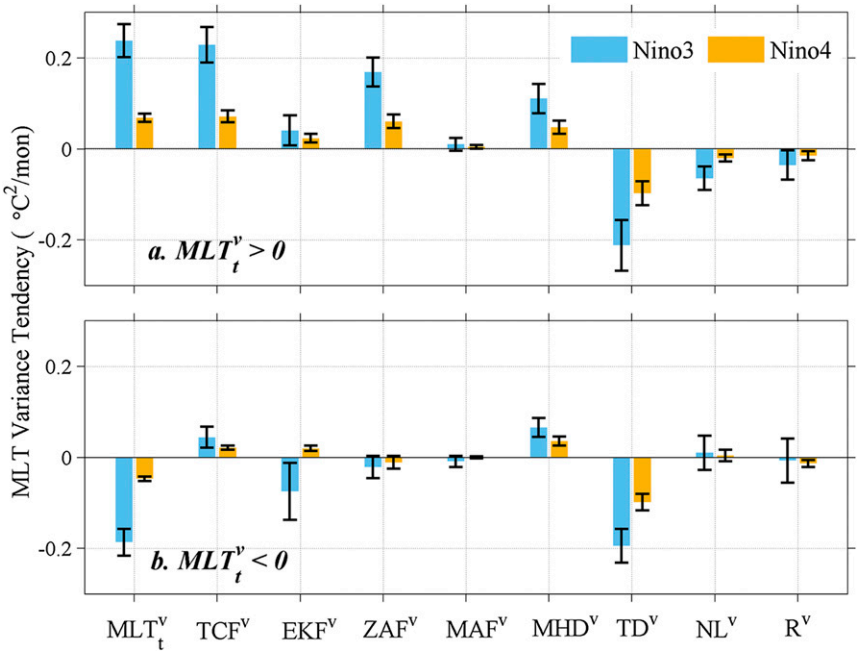

FIG. 6. Averages of individual temperature variance budget terms ($°C^2$ $month^{-1}$) in the Niño-3 and Niño-4 regions over the 30-yr period. Averages are calculated separately over (a) growing phase (shown as $MLT_t^v > 0$) and (b) decaying phase ($MLT_t^v < 0$). Error bars are shown for 95% confidence levels based on the seven different products.

different feedback terms, is distinct from that of Boucharel et al. (2015), who omitted the MLT^v tendency term in their diagnostic equation to study decadal variations of ENSO properties averaged over complete cycles.

In Fig. 6, the temperature variance tendency term is much larger in the Niño-3 versus in the Niño-4 region, as expected. Positive MLT_t^v values are also larger in amplitude than negative values, indicating a more rapid growth rate than decay rate for both El Niño and La Niña events. In the variance growth phase, TCF^v is the largest of the positive feedbacks in the Niño-3 region, followed by ZAF^v. In the Niño-4 region on the other hand, ZAF^v is of comparable magnitude to TCF^v. In the variance decay phase, positive feedbacks associated with TCF^v and ZAF^v decrease, leaving MHD^v as the largest positive feedback. The TD^v is the largest negative feedback term during both phases in both regions; MAF^v is the smallest term in both regions.

c. *Temperature variance budget changes between the 1980s–90s and 2000s*

To investigate how various terms in the temperature variance budget changed between the latter decades of the twentieth century and the first decade of the twenty-first century, we averaged each term in the two periods P1 and P2 for each individual model product (Fig. 7) and for the ensemble means (Fig. 8). Compared to P1, both the net and the positive temperature variance tendency MLT_t^v decrease in the Niño-3 region and increase in Niño-4 in P2, which is consistent with the shift toward more CP El Niños in the first decade of the twenty-first century.

During the variance growth phase (Fig. 8a), most terms (both positive and negative values) decreased from P1 to P2 in the Niño-3 region. Among the positive terms, TCF^v is both the largest and shows the biggest reduction from P1 to P2, consistent with a weakening of the thermocline feedback, as described in LM2014. The value of ZAF^v is the second largest positive term in Niño-3 and also decreases on average from P1 to P2 (Fig. 8), but less so than TCF^v. Thus, positive values of ZAF^v become comparable to those of TCF^v during P2 in the Niño-3 region. The value of MHD^v decreases as well from P1 to P2, and the decrease in the sum of ZAF^v and MHD^v is comparable to that of the decrease in TCF^v.

For the Niño-4 region, ensemble average differences in positive feedbacks from P1 to P2 during the growing phase are smaller than in Niño-3 (Fig. 8a). There is a slight reduction in TCF^v evident in all seven

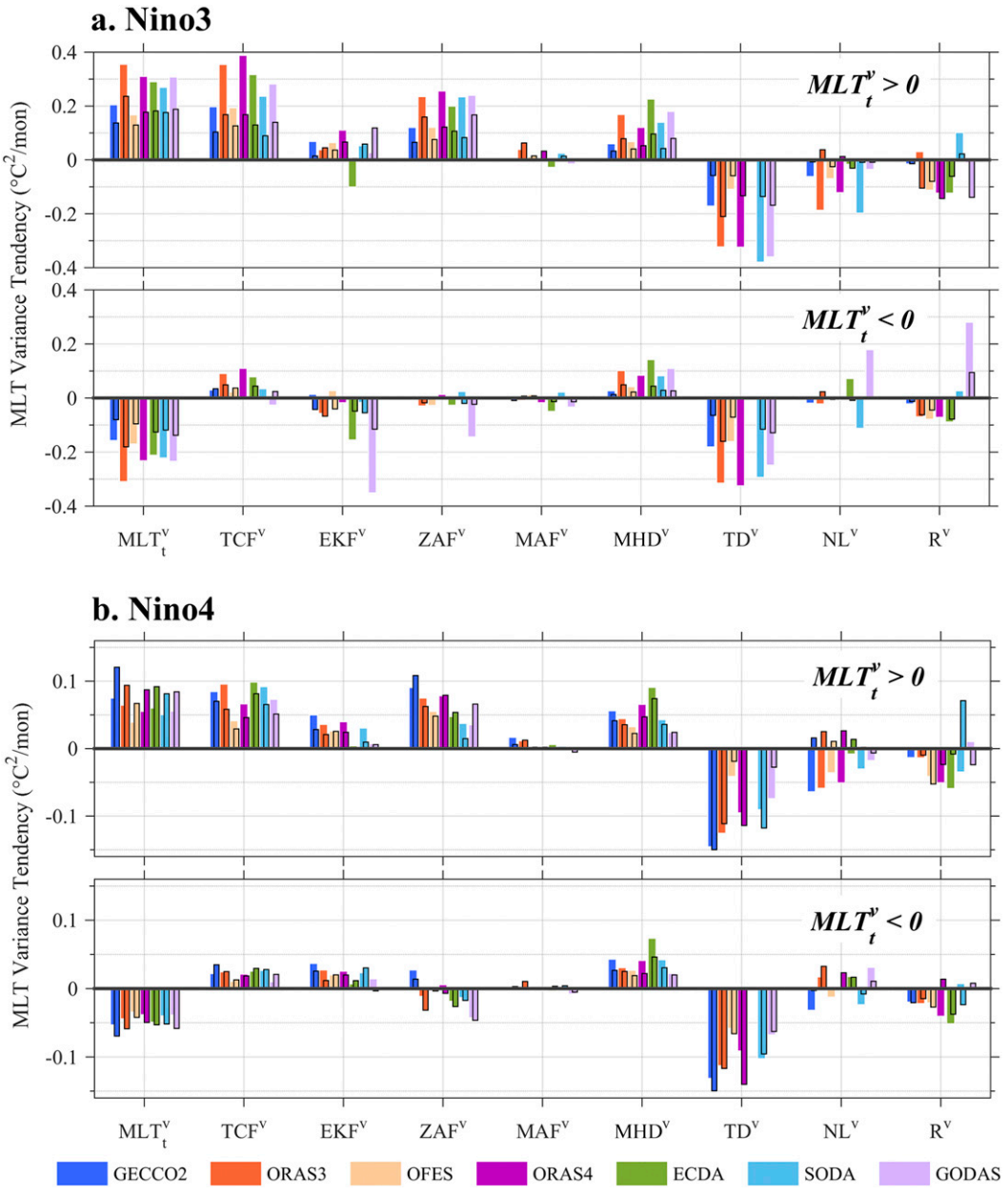

FIG. 7. Averages of individual temperature variance budget terms (°C^2 month^{-1}) for two periods, P1 (bars without black edge) and P2 (bars with black edge), in the (a) Niño-3 and (b) Niño-4 regions. Averages are calculated over the growing phase ($MLT_t^v > 0$) and decaying phase ($MLT_t^v < 0$) of the MLT variance separately.

model products, which, although small, is probably significant (Fig. 7b). Notably, TCF^v is also important in generating MLT variance in both the variance growth and decay phases in the Niño-4 region during both periods, consistent with the results of Ren and Jin (2013). The value of ZAF^v increases in some model products but decreases in others (Fig. 7b), remaining relatively unchanged from P1 to P2 in the ensemble mean (Fig. 8a).

Nonlinearity as a sink of variance decreased significantly from the P1 to P2 in both regions during the variance growth phase. This decreased NL^v in the Niño-3 region is related to a weaker ENSO cycle in P2, since nonlinearity in general decreases as the amplitude of events decreases. In the Niño-4 region, the nonlinearity in P1 results mainly from variations at the bottom of the mixed layer (not shown). This nonlinearity weakens in P2 most likely because the

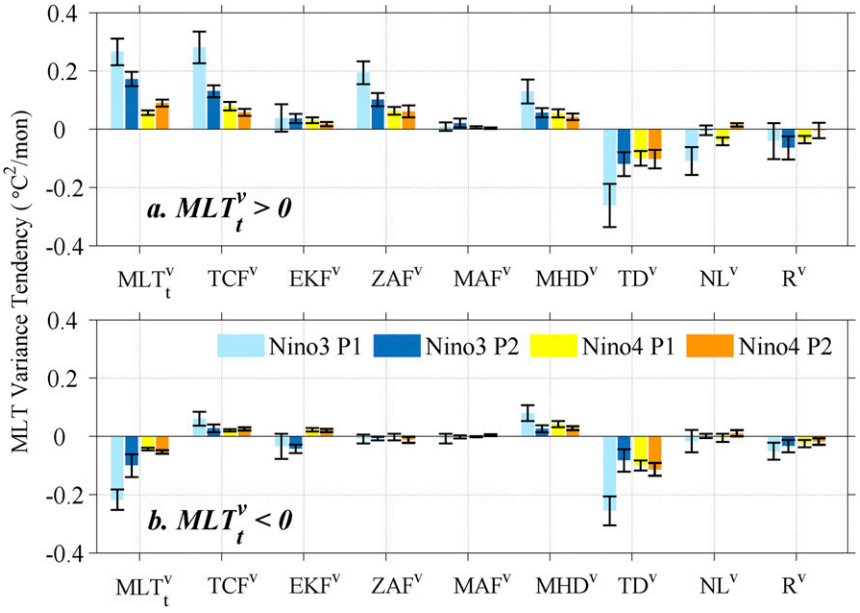

FIG. 8. As in Fig. 7, but for ensemble means: (a) variance growing phase and (b) variance decaying phase. Error bars are for 95% confidence limits based on the seven different model products.

thermocline is deeper in P2 than in P1 in the Niño-4 region as a result of the stronger trade winds in P1 (Fig. 2). Thus, at our fixed 50-m depth used for the temperature variance analysis, the vertical temperature gradients and temperature variations are weaker in P2, resulting in weaker nonlinearity. The changes in R^v from P1 to P2 among various products in both regions is highly variable (Fig. 7), and, given that variability, there is no clear change in the ensemble means from P1 to P2 (Fig. 8a).

With respect to negative tendencies, thermal damping TD^v is in general the most significant sink of variance in both regions during growth and decay phases. It undergoes substantial reduction in the Niño-3 region from P1 to P2 in all the model products and in the ensemble mean, consistent with the reduction in the amplitude of Niño-3 MLT anomalies from P1 to P2 (Fig. 7a). During the variance decay phase (Fig. 8b), both TCF^v and MHD^v undergo substantial reduction from P1 to P2, making the weaker TD^v more effective at damping variance than it would otherwise be.

We thus conclude that Niño-3 variance decreased from P1 to P2, mostly due to a reduced positive TCF^v, consistent with LM2014. The increase in Niño-4 variance between P1 and P2 is related to the weaker variance sink from nonlinearity in P2, since other positive feedbacks did not strengthen overall and thermal damping did not significantly weaken. In both regions, the TCF^v weakened relative to the ZAF^v in P2 compared to P1, such that the latter became relatively more important than TCF^v in generating ENSO SST variance. These results are consistent with the shift from EP to CP El Niños between the two time periods. They also offer a more precise determination of regional variations in feedback terms than the BJ index method and allow for greater resolution of the zonal variations in key feedback terms between P1 and P2. Another advantage of the temperature variance approach is described in the following section, where we examine aspects of TCF^v in the context of the recharge oscillator theory (Jin 1997a,b).

d. A temperature variance budget perspective on recharge oscillator dynamics

The thermocline feedback has traditionally been viewed as a positive feedback on ENSO SST anomaly growth in most previous heat budget studies (e.g., Jin and Neelin 1993; Jin and An 1999; Jin et al. 2006; LM2014; Boucharel et al. 2015). However, from our temperature variance budget analysis, it is evident that there are times when this feedback is clearly negative (Figs. 4 and 5). These periods of negative feedback occur mostly during decaying phases of El Niño and La Niña, suggestive of the role of the thermocline feedback in

terminating ENSO events (see also Kug et al. 2009). According to recharge oscillator theory (Jin 1997a,b), the TCF affects both ENSO anomaly growth and phase transition. Anomaly growth in this theory is influenced by the anomalous zonal tilt of the thermocline, while transitions from one phase of ENSO to another are linked to variations in zonal mean thermocline depth anomalies across the Pacific basin. In this section, we apply the temperature variance budget formalism to the ECMWF ORAS3, which is representative of other reanalysis products in our ensemble, to quantitatively diagnose the components of the thermocline feedback in the Niño-3 region where this feedback is strongest.

Variability in the thermocline feedback is controlled by variability in δT_B: namely, the difference between temperature at 50-m depth and the temperature averaged in the surface layer, based on (2) and the equivalent expression in the variance budget (see the appendixes). Temperature variations at 50-m depth are induced by changes in thermocline depth and are typically larger than the variations in MLT. In the Niño-3 region, thermocline depth anomalies result from both thermocline tilt and also the mean zonally averaged thermocline depth across the entire basin. Here we average h20 anomalies in both the eastern box (5°S–5°N, 150°–90°W) and the western box (5°S–5°N, 150°E–150°W), designated as $\mathrm{h20}_E$ and $\mathrm{h20}_W$, respectively. The zonal mean thermocline depth is then defined as $\mathrm{h20}_{\mathrm{ZM}} = (\mathrm{h20}_E + \mathrm{h20}_W)/2$ and the thermocline tilt as $\mathrm{h20}_{\mathrm{ZG}} = (\mathrm{h20}_E - \mathrm{h20}_W)/2$. Note the eastern box is also the Niño-3 region, so the thermocline anomalies in Niño-3 can be derived as $\mathrm{h20}_E = \mathrm{h20}_{\mathrm{ZM}} + \mathrm{h20}_{\mathrm{ZG}}$.

As expected, temperature difference between the bottom interface and mixed layer average in the Niño-3 region (defined as $\delta T_{B,E}$) is highly correlated and in phase with thermocline depth, with a zero lag correlation coefficient of 0.95 (Fig. 9). Thus, the relationship between these two variables can be expressed as $\delta T_{B,E} = \alpha \mathrm{h20}_E$, where α is the linear regression coefficient. We can define $\mathrm{h20}_E = \mathrm{h20}_{\mathrm{ZM}} + \mathrm{h20}_{\mathrm{ZG}}$ so that $\delta T_B = \alpha \mathrm{h20}_{\mathrm{ZM}} + \alpha \mathrm{h20}_{\mathrm{ZG}}$. Then we can separate TCF^{v} into two parts:

$$\mathrm{TCF}^{v} = \mathrm{TCF}^{v}_{\mathrm{ZM}} + \mathrm{TCF}^{v}_{\mathrm{ZG}}, \tag{5}$$

where $\mathrm{TCF}^{v}_{\mathrm{ZM}} = (\alpha/B)\iint \overline{w_B}\,\mathrm{h20}'_{\mathrm{ZM}}\,T'_{\mathrm{ave}}\,dx\,dy$ and $\mathrm{TCF}^{v}_{\mathrm{ZG}} = (\alpha/B)\iint \overline{w_B}\,\mathrm{h20}'_{\mathrm{ZG}}\,T'_{\mathrm{ave}}\,dx\,dy$. We find that $\mathrm{TCF}^{v}_{\mathrm{ZG}}$ always acts as positive feedback (Fig. 10), while $\mathrm{TCF}^{v}_{\mathrm{ZM}}$ is positive during developing phases of ENSO events, but negative during decay phases. For example, after an El Niño peaks, zonal-mean thermocline across equatorial Pacific shoals rapidly, discharging heat to off-equator regions. At the same time, climatological upwelling pumps anomalous cold subsurface thermocline water upward to the surface while the surface temperatures are still anomalously high. Thus, during the decay phase of an El Niño, $\mathrm{TCF}^{v}_{\mathrm{ZM}}$ is a negative feedback that helps to terminate the event. As the zonal-mean thermocline continues to shoal, the system transitions from a warm El Niño event to a cold La Niña event, with the TCF^{v} becoming a positive feedback during the developing phase of La Niña. Similar phasing of feedbacks is involved in the transition from La Niña to El Niño events.

Associated with the decrease in TCF^{v} from P1 to P2, we see both $\mathrm{TCF}^{v}_{\mathrm{ZG}}$ and $\mathrm{TCF}^{v}_{\mathrm{ZM}}$ are weaker in the 2000s in both growing and decaying phases (Fig. 10b). In the growth phase, the significant reduction of $\mathrm{TCF}^{v}_{\mathrm{ZM}}$ suggests reduced effectiveness of warm water volume as a predictor for interannual SST anomalies (McPhaden 2012). The decrease of $\mathrm{TCF}^{v}_{\mathrm{ZM}}$ from P1 to P2 in the decaying phase is consistent with a reduced efficiency of recharge oscillator dynamics in the termination of CP El Niño events, which dominate this decade (Kug et al. 2009).

4. Summary

We assessed the twenty-first-century shift in ENSO SST variability, characterized by a significant decrease in the magnitude of interannual SST anomalies in the eastern equatorial Pacific but a slight increase in anomalous SST variability in the central equatorial Pacific. To quantify the roles of various physical processes in affecting this shift, we examined both the temperature budget and the temperature variance budget in the mixed layer of the Niño-3 and Niño-4 regions for the time periods 1980–99 (P1) and 2000–10 (P2) using seven ocean model products. We found a prominent reduction during the growth phase of ENSO events in the thermocline feedback from P1 to P2 in the Niño-3 region, as well as reductions in the positive feedbacks associated with zonal advection and mean dynamical heating. Also evident was a weakening of thermodynamic damping and the variance sink due to nonlinearity. The net effect of all these changes was decreased interannual ENSO variability in the Niño-3 region in the 2000s relative to the 1980s and 1990s. In the Niño-4 region, there was little notable difference in most feedbacks from P1 to P2, except for slight weakening of the thermocline feedback and a reduction in the damping effect of nonlinearity during the growth phase. These decadal tendencies are consistent with the shift from predominantly EP El Niño variability in P1 to CP El Niño variability in P2.

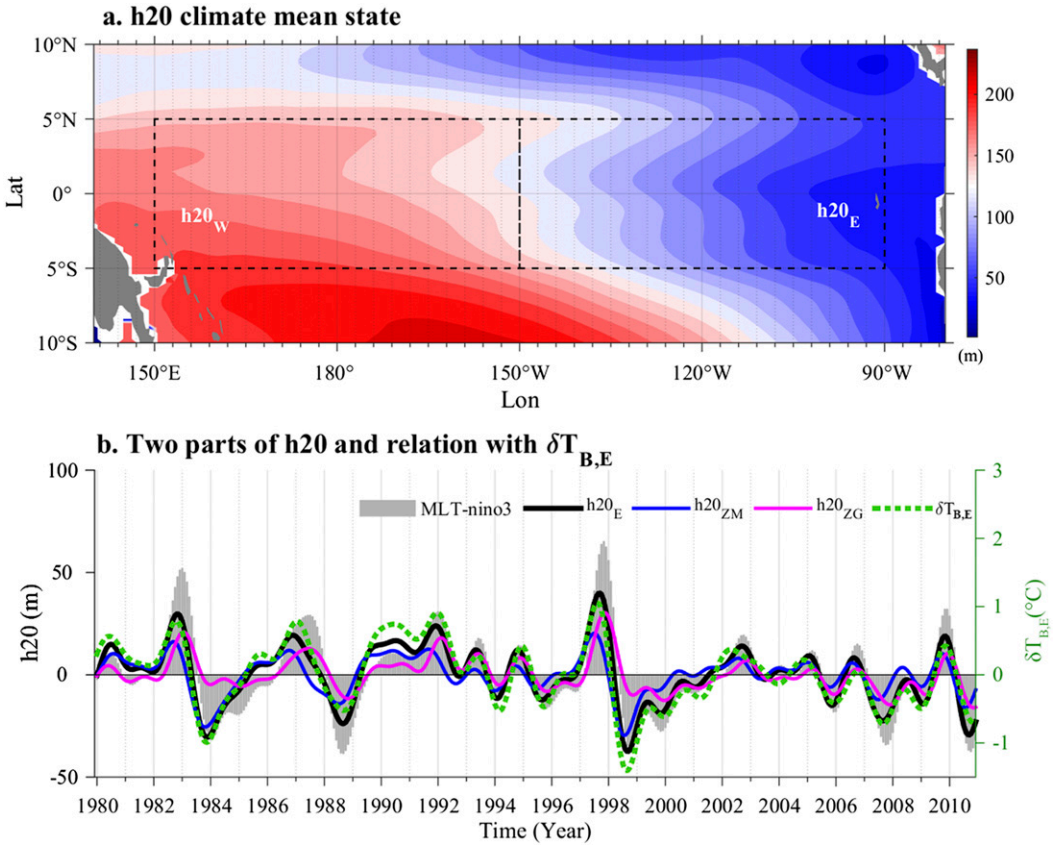

FIG. 9. Decomposition of h20 anomalies. (a) Mean state of h20 during 1980–2010, where regions to calculate the zonal gradient thermocline anomaly ($h20_{ZG}$) and the zonal mean thermocline anomaly ($h20_{ZM}$) are labeled by two dashed boxes $h20_W$ and $h20_E$. (b) Interannual anomalies of h20 and temperature difference between the bottom interface and mixed layer average ($\delta T_{B,E}$). Note the $\delta T_{B,E}$ (green dotted line), which is a measure of the thermocline feedback, and h20 in the Niño-3 region ($h20_E$) are highly correlated, with a correlation coefficient of 0.95.

We also examined the implications of recharge oscillator theory and how it is reflected in the temperature and temperature variance budgets during P1 and P2. During the growth phase of ENSO, a significant reduction of TCF^{v}_{ZM} from P1 to P2 in the Niño-3 region suggests reduced effectiveness of warm water volume as a predictor for interannual SST anomalies (McPhaden 2012). The weakening of this process in the decay phase of ENSO indicates a reduced efficiency of recharge oscillator dynamics in the termination of CP El Niño events.

The shift in maximum SST variability from the Niño-3 region to the Niño-4 region in the twenty-first century is evident in various ocean products. From the perspective of a temperature variance budget, we confirmed the results of LM2014 as to why Niño-3 SST variability decreased in the 2000s and also determined with more precise localization what dynamical processes contributed to the greatly decreased SST variability in the Niño-3 region. In addition, our temperature variance methodology allows us to describe within a consistent framework how both the positive and negative thermocline feedbacks operate in the context of recharge oscillator theory.

While we have diagnosed processes responsible for the observed patterns of equatorial Pacific SST variability in the 1980s–90s and 2000s separately, we have not addressed the reasons why these changes have occurred. It could be that decadal changes in background conditions between these two periods favored the development of EP El Niños in the 1980s–90s and CP El Niños in the 2000s (Choi et al. 2011; Chung and Li 2013; Xiang et al. 2013). Using model simulations, Choi et al. (2011) pointed out that a high occurrence of CP El Niños is related to strengthened trade winds and stronger zonal mean surface temperature gradients in the equatorial Pacific. Chung and Li (2013) further analyzed the relationship between the mean state and El Niño type on interdecadal time scales and found a steepening zonal SST gradient in the 2000s favored CP El Niños due to the westward shift of anomalous convection. Based on

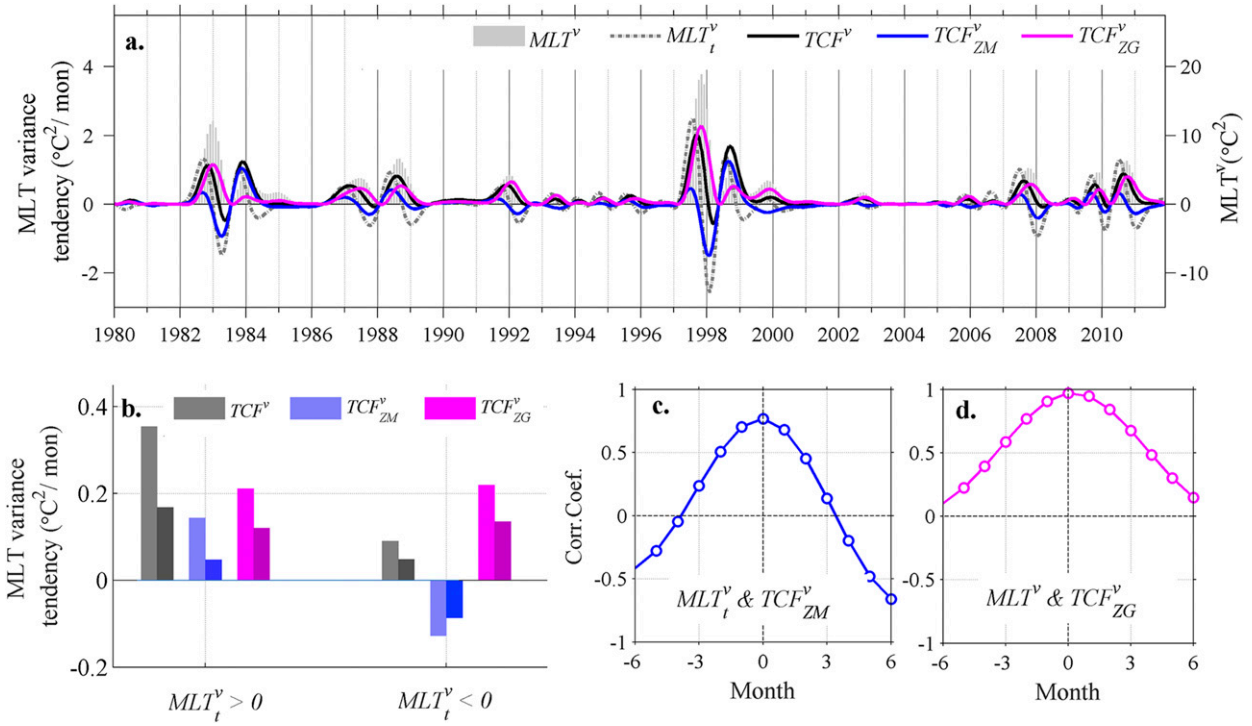

FIG. 10. Decomposition of the TCF^{v} in the Niño-3 region based on ORAS3. (a) Time series of total TCF^{v}, TCF^{v}_{ZM}, TCF^{v}_{ZG}, MLT^{v} (gray bars), and MLT^{v}_{t}. (b) Averages of TCF^{v} and its two components over the two periods P1 and P2, darker colors represent P2. (c) Lead–lag correlation between MLT^{v}_{t} and TCF^{v}_{ZM}. (d) Lead–lag correlation between MLT^{v} and TCF^{v}_{ZG}.

numerical model experiments, Xiang et al. (2013) proposed that the more frequent occurrence of CP El Niños in the 2000s arose from an enhanced subsidence and surface divergence in the central Pacific based on numerical model experiments. Conversely, the changes in ENSO statistics may be the result of random variations in the climate system that then project onto mean state changes (Rodgers et al. 2004; Choi et al. 2012; McPhaden et al. 2011). This larger question of what ultimately accounts for the observed decadal changes, although very important, is beyond the scope of the present study.

Recently, a major El Niño occurred in the tropical Pacific in 2015/16 (McPhaden 2015). Initial development of this El Niño, which is not represented in our model products that extend only to 2010, resembled an EP-type El Niño, with largest SST and thermocline depth variations in the eastern Pacific. Whether this event signals a decadal shift toward more frequent EP versus CP El Niños as in the 1980s and 1990s remains to be seen.

Acknowledgments. This research was carried out while the first author had a coeducate Ph.D. program at NOAA/PMEL. The authors express their sincere gratitude to Dr. Fan Wang from the Institute of Oceanology of CAS, the China Scholarship Council, and NOAA/PMEL for supporting this effort. We also acknowledge the very thoughtful and constructive critiques of three anonymous reviewers and the editor in improving the quality of this manuscript. We thank Hamburg University, the ECMWF, University of Maryland, GFDL, NOAA, and JAMSTEC APL for their valuable model products and data. This work was supported by the National Basic Research Program of China (973Program; 2012CB417401) and the CAS Strategic Priority Research Program (No. XDA11010204).

APPENDIX A

Volumetric Temperature Budget Formulation

The schematic box shown in Fig. A1 is used to define the following formulation.

$$\mathrm{MLT}_t = T_{\mathrm{advB}} + T_{\mathrm{advW}} + T_{\mathrm{advE}} + T_{\mathrm{advS}} + T_{\mathrm{advN}} + T_{\mathrm{surf}} + R, \tag{A1}$$

where

$$\mathrm{MLT}_t = \partial T_{\mathrm{ave}}/\partial t;$$

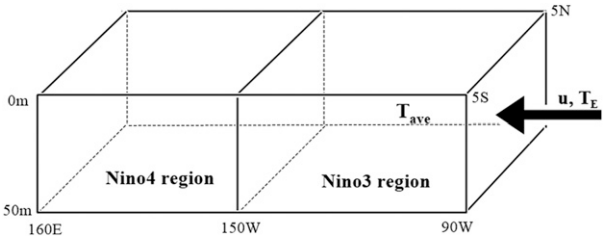

FIG. A1. Schematic plot to indicate the boxes over Niño-3 and Niño-4 used for the heat budget analysis.

$$T_{\text{advB}} = \frac{1}{B}\iint w_B \delta T_B \, dx\, dy, \quad \text{where} \quad \delta T_B = T_B - T_{\text{ave}};$$

$$T_{\text{advW}} = \frac{1}{B}\iint u_W \delta T_W \, dy\, dz;$$

$$T_{\text{advE}} = \frac{1}{B}\iint -u_E \delta T_E \, dy\, dz;$$

$$T_{\text{advS}} = \frac{1}{B}\iint v_S \delta T_S \, dx\, dz;$$

$$T_{\text{advN}} = \frac{1}{B}\iint -v_N \delta T_N \, dx\, dz; \quad \text{and}$$

$$T_{\text{surf}} = \frac{1}{\rho c_p B}\iint q_{\text{net}} \, dx\, dy.$$

APPENDIX B

Temperature Budget Written in Terms of Individual Feedback Terms

We can define each variable as $M = \overline{M} + M'$, where M is MLT, ocean velocity, or another variable, and M' denotes monthly anomaly. Then, for anomalies, we can write (dropping the primes for simplicity)

$$\text{MLT}_t = \text{TCF} + \text{EKF} + \text{ZAF} + \text{MAF} + \text{MHD} + \text{TD} + \text{NL} + R, \tag{B1}$$

where

$$\text{MLT}_t = \partial T'_{\text{ave}}/\partial t,$$

$$\text{TCF} = \frac{1}{B}\iint \overline{w_B}\delta T'_B \, dx\, dy,$$

$$\text{EKF} = \frac{1}{B}\iint w'_B \overline{\delta T_B} \, dx\, dy,$$

$$\text{ZAF} = \frac{1}{B}\iint (u'_W \overline{\delta T_W} - u'_E \overline{\delta T_E}) \, dy\, dz,$$

$$\text{MAF} = \frac{1}{B}\iint (v'_S \overline{\delta T_S} - v'_N \overline{\delta T_N}) \, dx\, dz,$$

$$\text{MHD} = \frac{1}{B}\left[\iint (\overline{u_W}\delta T'_W - \overline{u_E}\delta T'_E) \, dy\, dz + \iint (\overline{v_S}\delta T'_S - \overline{v_N}\delta T'_N) \, dx\, dz\right],$$

$$\text{NL} = \frac{1}{B}\left[\iint (u'_W \delta T'_W - u'_E \delta T'_E) \, dy\, dz + \iint (v'_S \delta T'_S - v'_N \delta T'_N) \, dx\, dz + \iint w'_B \delta T'_B \, dx\, dy\right], \quad \text{and}$$

$$\text{TD} = \frac{1}{\rho c_p B}\iint q'_{\text{net}} \, dx\, dy.$$

APPENDIX C

Temperature Variance Budget Written in Terms of Individual Feedback Terms

Analogous to (B1), we can write the temperature variance budget as

$$\text{MLT}^v_t = \text{TCF}^v + \text{EKF}^v + \text{ZAF}^v + \text{MAF}^v + \text{MHD}^v + \text{TD}^v + \text{NL}^v + R^v, \tag{C1}$$

where

$$\text{MLT}^v_t = \frac{1}{2}\partial (T'_{\text{ave}})^2/\partial t = \frac{1}{2}(\text{MLT}^v)_t,$$

$$\text{TCF}^v = \frac{1}{B}\iint \overline{w_B}\delta T'_B T'_{\text{ave}} \, dx\, dy,$$

$$\text{EKF}^v = \frac{1}{B}\iint w'_B \overline{\delta T_B} T'_{\text{ave}} \, dx\, dy,$$

$$\text{ZAF}^v = \frac{1}{B}\iint (u'_W \overline{\delta T_W} - u'_E \overline{\delta T_E}) T'_{\text{ave}} \, dy\, dz,$$

$$\text{MAF}^v = \frac{1}{B}\iint (v'_S \overline{\delta T_S} - v'_N \overline{\delta T_N}) T'_{\text{ave}} \, dx\, dz,$$

$$\text{MHD}^v = \frac{1}{B}\left[\iint (\overline{u_W}\delta T'_W - \overline{u_E}\delta T'_E) T'_{\text{ave}} \, dy\, dz + \iint (\overline{v_S}\delta T'_S - \overline{v_N}\delta T'_N) T'_{\text{ave}} \, dx\, dz\right],$$

$$\text{NL}^v = \frac{1}{B}\left[\iint (u'_W \delta T'_W - u'_E \delta T'_E) T'_{\text{ave}} \, dy\, dz + \iint (v'_S \delta T'_S - v'_N \delta T'_N) T'_{\text{ave}} \, dx\, dz + \iint w'_B \delta T'_B T'_{\text{ave}} \, dx\, dy\right], \quad \text{and}$$

$$\text{TD}^v = \frac{1}{\rho c_p B}\iint q'_{\text{net}} T'_{\text{ave}} \, dx\, dy.$$

REFERENCES

An, S.-I., F.-F. Jin, and I.-S. Kang, 1999: The role of zonal advection feedback in phase transition and growth of ENSO in the Cane–Zebiak model. *J. Meteor. Soc. Japan*, **77**, 1151–1160.

Ashok, H., and T. Yamagata, 2009: Climate change: The El Niño with a difference. *Nature*, **461**, 481–484, doi:10.1038/461481a.

Ashok, K., S. K. Behera, S. A. Rao, H. Weng, and T. Yamagata, 2007: El Niño Modoki and its possible teleconnection. *J. Geophys. Res.*, **112**, C11007, doi:10.1029/2006JC003798.

Balmaseda, M. A., A. Vidard, and D. L. T. Anderson, 2008: The ECMWF Ocean Analysis System: ORA-S3. *Mon. Wea. Rev.*, **136**, 3018–3034, doi:10.1175/2008MWR2433.1.

——, K. Mogensen, and A. T. Weaver, 2013: Evaluation of the ECMWF Ocean Reanalysis System ORAS4. *Quart. J. Roy. Meteor. Soc.*, **139**, 1132–1161, doi:10.1002/qj.2063.

Barnston, A. G., M. K. Tippett, M. L. L'Heureux, S. Li, and D. G. DeWitt, 2012: Skill of real-time seasonal ENSO model predictions during 2002–11: Is our capability increasing? *Bull. Amer. Meteor. Soc.*, **93**, 631–651, doi:10.1175/BAMS-D-11-00111.1.

Behringer, D., and Y. Xue, 2004: Evaluation of the global ocean data assimilation system at NCEP: The Pacific Ocean. *Eighth Symp. on Integrated Observing and Assimilation Systems for Atmosphere, Oceans, and Land Surface*, Seattle, WA, Amer. Meteor. Soc., 2.3. [Available online at https://ams.confex.com/ams/pdfpapers/70720.pdf.]

Boucharel, J., A. Timmermann, A. Santoso, M. H. England, F. F. Jin, and M. A. Balmaseda, 2015: A surface layer variance heat budget for ENSO. *Geophys. Res. Lett.*, **42**, 3529–3537, doi:10.1002/2015GL063843.

Carton, J. A., and B. S. Giese, 2008: A reanalysis of ocean climate using Simple Ocean Data Assimilation (SODA). *Mon. Wea. Rev.*, **136**, 2999–3017, doi:10.1175/2007MWR1978.1.

Choi, J., S.-I. An, J.-S. Kug, and S.-W. Yeh, 2011: The role of mean state on changes in El Niño's flavor. *Climate Dyn.*, **37**, 1205–1215, doi:10.1007/s00382-010-0912-1.

——, ——, and S.-W. Yeh, 2012: Decadal amplitude modulation of two types of ENSO and its relationship with the mean state. *Climate Dyn.*, **38**, 2631–2644, doi:10.1007/s00382-011-1186-y.

Chung, P.-H., and T. Li, 2013: Interdecadal relationship between the mean state and El Niño types. *J. Climate*, **26**, 361–379, doi:10.1175/JCLI-D-12-00106.1.

Dawdy, D., and N. Matalas, 1964: Statistical and probability analysis of hydrologic data. Part III: Analysis of variance, covariance and time series. *Handbook of Applied Hydrology, A Compendium of Water-Resources Technology*, V. T. Chow, Ed., McGraw-Hill Book Company, 68–90.

Derber, J. C., and A. Rosati, 1989: A global oceanic data assimilation system. *J. Phys. Oceanogr.*, **19**, 1333–1347, doi:10.1175/1520-0485(1989)019<1333:AGODAS>2.0.CO;2.

Dewitte, B., S.-W. Yeh, and S. Thual, 2013: Reinterpreting the thermocline feedback in the western-central equatorial Pacific and its relationship with the ENSO modulation. *Climate Dyn.*, **41**, 819–830, doi:10.1007/s00382-012-1504-z.

Graham, F. S., J. N. Brown, C. Langlais, S. J. Marsland, A. T. Wittenberg, and N. J. Holbrook, 2014: Effectiveness of the Bjerknes stability index in representing ocean dynamics. *Climate Dyn.*, **43**, 2399–2414, doi:10.1007/s00382-014-2062-3.

Guan, C., Y.-L. Chen, and F. Wang, 2013: Seasonal variability of zonal heat advection in the mixed layer of the tropical Pacific. *Chin. J. Oceanol. Limnol.*, **31**, 1356–1367, doi:10.1007/s00343-014-3019-4.

Haan, C. T., 2002: *Statistical Methods in Hydrology*. 3rd ed. Iowa State University Press, 378 pp.

Horii, T., I. Ueki, and K. Hanawa, 2012: Breakdown of ENSO predictors in the 2000s: Decadal changes of recharge/discharge SST phase relation and atmospheric intraseasonal forcing. *Geophys. Res. Lett.*, **39**, L10707, doi:10.1029/2012GL051740.

Hu, Z.-Z., A. Kumar, H. L. Ren, H. Wang, M. L'Heureux, and F. F. Jin, 2013: Weakened interannual variability in the tropical Pacific Ocean since 2000. *J. Climate*, **26**, 2601–2613, doi:10.1175/JCLI-D-12-00265.1.

Huang, B., and Coauthors, 2015: Extended Reconstructed Sea Surface Temperature version 4 (ERSST.v4). Part I: Upgrades and intercomparison. *J. Climate*, **28**, 911–930, doi:10.1175/JCLI-D-14-00006.1.

Jin, F.-F., 1997a: An equatorial ocean recharge paradigm for ENSO. Part I: Conceptual model. *J. Atmos. Sci.*, **54**, 811–829, doi:10.1175/1520-0469(1997)054<0811:AEORPF>2.0.CO;2.

——, 1997b: An equatorial ocean recharge paradigm for ENSO. Part II: A stripped-down coupled model. *J. Atmos. Sci.*, **54**, 830–846, doi:10.1175/1520-0469(1997)054<0830:AEORPF>2.0.CO;2.

——, and J. D. Neelin, 1993: Modes of interannual tropical ocean–atmosphere interaction—A unified view. Part I: Numerical results. *J. Atmos. Sci.*, **50**, 3477–3503, doi:10.1175/1520-0469(1993)050<3477:MOITOI>2.0.CO;2.

——, and S.-I. An, 1999: Thermocline and zonal advective feedbacks within the equatorial ocean recharge oscillator model for ENSO. *Geophys. Res. Lett.*, **26**, 2989–2992, doi:10.1029/1999GL002297.

——, ——, A. Timmermann, and J. Zhao, 2003: Strong El Niño events and nonlinear dynamical heating. *Geophys. Res. Lett.*, **30**, 1120, doi:10.1029/2002GL016356.

——, S. T. Kim, and L. Bejarano, 2006: A coupled-stability index for ENSO. *Geophys. Res. Lett.*, **33**, L23708, doi:10.1029/2006GL027221.

Kao, H.-Y., and J.-Y. Yu, 2009: Contrasting eastern-Pacific and central-Pacific types of El Niño. *J. Climate*, **22**, 615–632, doi:10.1175/2008JCLI2309.1.

Kim, S.-B., T. Lee, and I. Fukumori, 2007: Mechanisms controlling the interannual variations of mixed layer temperature averaged over the Niño-3 region. *J. Climate*, **20**, 3822–3843, doi:10.1175/JCLI4206.1.

Köhl, A., and D. Stammer, 2008: Variability of the meridional overturning in the North Atlantic from the 50-yr GECCO state estimation. *J. Phys. Oceanogr.*, **38**, 1913–1930, doi:10.1175/2008JPO3775.1.

Kug, J. S., F.-F. Jin, and S.-I. An, 2009: Two types of El Niño events: Cold tongue El Niño and warm pool El Niño. *J. Climate*, **22**, 1499–1515, doi:10.1175/2008JCLI2624.1.

——, J. Choi, S.-I. An, F.-F. Jin, and A. T. Wittenberg, 2010: Warm pool and cold tongue El Niño events as simulated by the GFDL 2.1 coupled GCM. *J. Climate*, **23**, 1226–1239, doi:10.1175/2009JCLI3293.1.

Larkin, N. K., and D. E. Harrison, 2005a: On the definition of El Niño and associated seasonal average U.S. weather anomalies. *Geophys. Res. Lett.*, **32**, L13705, doi:10.1029/2005GL022738.

——, and ——, 2005b: Global seasonal temperature and precipitation anomalies during El Niño autumn and winter. *Geophys. Res. Lett.*, **32**, L16705, doi:10.1029/2005GL022860.

Lee, T., and M. J. McPhaden, 2010: Increasing intensity of El Niño in the central-equatorial Pacific. *Geophys. Res. Lett.*, **37**, L14603, doi:10.1029/2010GL044007.

——, I. Fukumori, and B. Tang, 2004: Temperature advection: Internal versus external processes. *J. Phys. Oceanogr.*, **34**, 1936–1944, doi:10.1175/1520-0485(2004)034<1936:TAIVEP>2.0.CO;2.

Lübbecke, J. F., and M. J. McPhaden, 2014: Assessing the twenty-first-century shift in ENSO variability in terms of the Bjerknes stability index. *J. Climate*, **27**, 2577–2587, doi:10.1175/JCLI-D-13-00438.1.

Masumoto, Y., and Coauthors, 2004: A fifty-year eddy-resolving simulation of the world ocean—Preliminary outcomes of OFES (OGCM for the Earth Simulator). *J. Earth Simul.*, **1**, 35–56.

McPhaden, M. J., 2012: A 21st century shift in the relationship between ENSO SST and warm water volume anomalies. *Geophys. Res. Lett.*, **39**, L09706, doi:10.1029/2012GL051826.

——, 2015: Playing hide and seek with El Niño. *Nat. Climate Change*, **5**, 791–795, doi:10.1038/nclimate2775.

——, S. E. Zebiak, and M. H. Glantz, 2006: ENSO as an integrating concept in Earth science. *Science*, **314**, 1740–1745, doi:10.1126/science.1132588.

——, T. Lee, and D. McClurg, 2011: El Niño and its relationship to changing background conditions in the tropical Pacific Ocean. *Geophys. Res. Lett.*, **38**, L15709, doi:10.1029/2011GL048275.

Picaut, J., M. Ioualalen, C. Menkes, T. Delcroix, and M. J. McPhaden, 1996: Mechanism of the zonal displacements of the Pacific warm pool: Implications for ENSO. *Science*, **274**, 1486–1489, doi:10.1126/science.274.5292.1486.

Ren, H., and F. Jin, 2013: Recharge oscillator mechanisms in two types of ENSO. *J. Climate*, **26**, 6506–6523, doi:10.1175/JCLI-D-12-00601.1.

Rodgers, K. B., P. Friederichs, and M. Latif, 2004: Tropical Pacific decadal variability and its relation to decadal modulations of ENSO. *J. Climate*, **17**, 3761–3774, doi:10.1175/1520-0442(2004)017<3761:TPDVAI>2.0.CO;2.

Santoso, A., A. S. Gupta, and M. H. England, 2010: Genesis of Indian Ocean mixed layer temperature anomalies: A heat budget analysis. *J. Climate*, **23**, 5375–5403, doi:10.1175/2010JCLI3072.1.

Walters, R. A., and C. Heston, 1982: Removing tidal-period variations from time-series data using low-pass digital filters. *J. Phys. Oceanogr.*, **12**, 112–115, doi:10.1175/1520-0485(1982)012<0112:RTPVFT>2.0.CO;2.

Wen, C., A. Kumar, Y. Xue, and M. J. McPhaden, 2014: Changes in tropical Pacific thermocline depth and their relationship to ENSO after 1999. *J. Climate*, **27**, 7230–7249, doi:10.1175/JCLI-D-13-00518.1.

Woodruff, S. D., and Coauthors, 2011: ICOADS release 2.5: Extensions and enhancements to the surface marine meteorological archive. *Int. J. Climatol.*, **31**, 951–967, doi:10.1002/joc.2103.

Xiang, B., B. Wang, and T. Li, 2013: A new paradigm for the predominance of standing central Pacific warming after the late 1990s. *Climate Dyn.*, **41**, 327–340, doi:10.1007/s00382-012-1427-8.

Zhang, S., M. J. Harrison, A. Rosati, and A. T. Wittenberg, 2007: System design and evaluation of coupled ensemble data assimilation for global oceanic climate studies. *Mon. Wea. Rev.*, **135**, 3541–3564, doi:10.1175/MWR3466.1.

Zhang, X., and M. J. McPhaden, 2010: Surface layer heat balance in the eastern equatorial Pacific Ocean on interannual time scales: Influence of local versus remote wind forcing. *J. Climate*, **23**, 4375–4394, doi:10.1175/2010JCLI3469.1.